Published in final edited form as:

FASEB J. 2022 April ; 36(4): e22242. doi:10.1096/fj.202100901RRR.

Role of cellular retinol-binding protein, type 1 and retinoid homeostasis in the adult mouse heart: A multi-omic approach

Stephanie Zalesak-Kravec[1], **Weiliang Huang**[1], **Jace W. Jones**[1], **Jianshi Yu**[1], **Jenna Alloush**[1], **Amy E. Defnet**[1], **Alexander R. Moise**[2], **Maureen A. Kane**[1]

[1]Department of Pharmaceutical Sciences, School of Pharmacy, University of Maryland, Baltimore, Maryland, USA

[2]Medical Sciences Division, Northern Ontario School of Medicine, Sudbury, Ontario, Canada

Abstract

The main active metabolite of Vitamin A, *all-trans* retinoic acid (RA), is required for proper cellular function and tissue organization. Heart development has a well-defined requirement for RA, but there is limited research on the role of RA in the adult heart. Homeostasis of RA includes regulation of membrane receptors, chaperones, enzymes, and nuclear receptors. Cellular retinol-binding protein, type 1 (CRBP1), encoded by retinol-binding protein, type 1 *(Rbp1),* regulates RA homeostasis by delivering vitamin A to enzymes for RA synthesis and protecting it from non-specific oxidation. In this work, a multi-omics approach was used to characterize the effect of CRBP1 loss using the $Rbp1^{-/-}$ mouse. Retinoid homeostasis was disrupted in $Rbp1^{-/-}$ mouse heart tissue, as seen by a 33% and 24% decrease in RA levels in the left and right ventricles, respectively, compared to wild-type mice (WT). To further inform on the effect of disrupted RA homeostasis, we conducted high-throughput targeted metabolomics. A total of 222 metabolite and metabolite combinations were analyzed, with 33 having differential abundance between $Rbp1^{-/-}$ and WT hearts. Additionally, we performed global proteome profiling to further characterize the impact of CRBP1 loss in adult mouse hearts. More than 2606 unique proteins were identified, with 340 proteins having differential expression between $Rbp1^{-/-}$ and WT hearts. Pathway analysis performed on metabolomic and proteomic data revealed pathways related to cellular metabolism and cardiac metabolism were the most disrupted in $Rbp1^{-/-}$ mice. Together, these studies characterize the effect of CRBP1 loss and reduced RA in the adult heart.

Correspondence: Maureen A. Kane, Department of Pharmaceutical Sciences, School of Pharmacy, University of Maryland, 20 N. Pine St, Rm N731, Baltimore, MD 21201, USA, mkane@rx.umaryland.edu.
Stephanie Zalesak-Kravec, Weiliang Huang and Jace W. Jones are Co-first authors.

AUTHOR CONTRIBUTIONS

Maureen A. Kane designed research; Jenna Alloush, Jace W. Jones, Jianshi Yu, Amy E. Defnet, and Weiliang Huang performed research; Weiliang Huang, Jenna Alloush, Jace W. Jones, Jianshi Yu, Stephanie Zalesak-Kravec and Maureen A. Kane analyzed data; Stephanie Zalesak-Kravec, Weiliang Huang, Jace W. Jones, Alexander R. Moise, and Maureen A. Kane contributed to the writing and editing of the manuscript.

DISCLOSURES

The authors have no conflicts to declare.

SUPPORTING INFORMATION

Additional supporting information may be found in the online version of the article at the publisher's website.

Keywords

cellular retinol-binding protein; type 1; heart; mice; retinoic acid; retinoid metabolism

1 | INTRODUCTION

Vitamin A is an essential diet-derived nutrient that plays key roles in many biological processes, including proper cell function and tissue organization.[1] The main active metabolite of vitamin A is *all-trans* retinoic acid (RA), which is critical for nuclear-receptor mediated signaling for cell proliferation, differentiation, and apoptosis.[2,3] Proper RA levels regulate cell differentiation and remodeling and are essential for proper vertebrate embryo development.[4–11] In the developing heart, RA controls progenitor pool size, cardiomyocyte differentiation, inflow/outflow tract specification and determination, and epicardial control of myocardial compact zone growth and coronariogenesis.[4–6,10]

The role of RA has been extensively studied in the developing heart, and while it is known that the adult heart is responsive to RA,[12] research on this subject is limited. Dysregulated RA levels have been associated with many diseases, including heart disease.[3,13,14] In a study of patients with coronary artery disease, lower serum RA levels directly correlated with greater risk of mortality.[15] Vitamin A insufficiency in heart tissue increases ventricular remodeling after myocardial infarction (MI), which leads to worsening disease.[16] Several studies have also explored the use of RA as a therapeutic treatment after MI to prevent excessive ventricular remodeling that can result in hypertrophy.[5,7,10,17–21] When left unchecked, unnecessary cardiac remodeling, and subsequent hypertrophy, causes heart failure.

It is apparent that RA levels must be tightly regulated to maintain proper cardiac cellular function. In cells, RA biosynthesis is highly conserved between species and controlled through interactions of synthesizing and catabolizing enzymes, as well as through interactions with retinol- and RA-binding proteins.[1,22] Cellular retinol binding protein, type 1 (CRBP1), encoded by retinol-binding protein, type 1 *(Rbp1),* is a widely expressed intracellular chaperone protein for retinol and retinal.[23] CRBP1 regulates RA homeostasis by protecting retinol and retinal from non-specific oxidation and facilitating their delivery to the appropriate enzymes for RA biosynthesis.[2,24] CRBP1 is ubiquitously expressed in the body, including the heart,[25–29] and has also been shown to be affected by heart disease.[27–30] Decreased CRBP1 levels result in dysregulated RA biosynthesis because of the reduced retinol and retinal metabolism efficiency.[31,32] Therefore, an animal model of CRBP1 deficiency, such as *Rbp1*$^{-/-}$ mice, can provide insight into disrupted RA biosynthesis and signaling. In this study, *Rbp*$^{-/-}$ mice hearts are investigated via metabolomic and proteomic analyses to elucidate the role of CRBP1 and by extension RA metabolism in the adult heart using a systems biology approach.

2 | MATERIALS AND METHODS

2.1 | Mice and husbandry

Rbp1 knockout mice *(Rbp1*$^{-/-}$*)* in a C57BL/6 background and wild-type (WT; C57BL/6) mice were used according to institutional guidelines of the University of Maryland, Baltimore.[33] WT mice were purchased from Jackson Laboratories (Bar Harbor, ME, USA) and *Rbp1*$^{-/-}$ mice were bred in-house from breeders obtained from Pierre Chambon and Norbert Ghyselinck (Institut de Genetique et de Biologie Moleculaire et Cellulaire, Institut National de la Sante et de la Recherche Medicale, Illkirch, France). Mice were fed a chow diet *ad libitum* (Harlan Teklad Global; 18% protein extruded rodent diet no. 2018SX with the equivalent of 30 IU/g Vitamin A (retinyl acetate); Harlan Laboratories, Indianapolis, IN, USA). Mice were chosen at random and grouped according to age, sex, and genotype for retinoid, metabolite, and protein analyses.

2.2 | Retinoids

2.2.1 | Retinoid sample preparation—Each age-matched cohort (WT and *Rbp1*$^{-/-}$) had $n = 10$ female mice averaged 16.5 ± 4.0 months of age. The left and right ventricle were separated and snap frozen with liquid nitrogen and stored at −80°C until processed.

Samples were thawed on ice and placed into Kontes DUALL #21 glass homogenizer (DWK Life Sciences, LLC; Millville, NJ) on ice with 1.5 ml ice-cold 0.9% NaCl (normal saline). Tissue has homogenized and aliquoted for proteomics, retinoid extraction, and protein concentration as needed. The average tissue mass was 48.5 ± 29 mg and 47% of the homogenate was used for retinoid determination and 47% for proteomic analyses with the remainder used for protein determination. Only glass containers, pipettes, and syringes were used to handle retinoids. Extraction of retinoids was performed under yellow light using a two-step liquid-liquid extraction that has been described in detail previously using 4,4-dimethyl-RA as an internal standard for RA and retinyl acetate as an internal standard for retinol and total retinyl ester.[34–37]

2.2.2 | Retinoid sample analysis—RA was quantified by liquid chromatography-multistage tandem mass spectrometry (LC-MRM^3) which is an LC-MS/MS method utilizing two distinct fragmentation events for enhanced selectivity.[37] RA analysis was performed using a Shimadzu Prominence UFLC XR liquid chromatography system (Shimadzu, Columbia, MD) coupled to an AB Sciex 5500 QTRAP hybrid triple quadrupole mass spectrometer (AB Sciex, Framingham, MA) using atmospheric pressure chemical ionization (APCI) operated in positive ion mode as previously described in detail.[37] Retinol and RE were quantified via HPLC-UV using a Waters H-Class ACQUITY UPLC equipped with a PDA detector operated in single wavelength detection mode according to previously published methodology.[36,38] Retinoid levels were measured using $n = 10$ per group where the data is expressed as means ± SEM. Statistical significance was determined using an unpaired Student's *t*-test between groups with $p < .05$ considered significant. Prior to conducting the Student's *t*-test, analysis was performed to demonstrate that the data, which had been collected using a random sampling method, had normal distribution and equal variance.

2.3 | Metabolomics

2.3.1 | Metabolomics sample preparation—Each age-matched cohort (WT and *Rbp1*$^{-/-}$) had $n = 5$ male mice aged 10 weeks. Hearts were harvested and atria and ventricles were separated. Samples were flash frozen in liquid nitrogen and stored at −80°C until processed.

2.3.2 | High-throughput, targeted metabolomics—Targeted, quantitative metabolomics was performed using the Biocrates AbsoluteIDQ p180 kit (Biocrates, Life Science AG, Innsbruck, Austria). The AbsoluteIDQ p180 kit was prepared as described by the manufacturer. The assay quantifies or semiquantifies up to 188 metabolites from five metabolite classes: acylcarnitines, amino acids, biogenic amines, glycerophospholipids, sphingolipids, and hexose. Specific standards for each of the lipids and a subset of acylcarnitines are not commercially available, so their quantification is semi-quantitative. Internal standards, analyte derivatization and metabolite extraction are integrated into a 96-well plate kit. Metabolite detection is done via pre-selected selected reaction monitoring (SRM) transitions.

Heart tissue was homogenized in 85:15 (methanol:ethanol, v/v) with 5 mM PBS at a ratio of 5 mg/ml. After centrifugation, 20 µl of tissue homogenate was loaded onto the 96 well kit. 10 µl of internal standard cocktail was added followed by drying with nitrogen. A 5% solution of phenylisothiocyanate in ethanol:water:pyridine (1:1:1, v/v/v) was added for derivatization of biogenic amines and amino acids. Metabolite extraction was achieved with 5 mM ammonium acetate in methanol. Analyses were performed according to the manufacturer's instructions on a tandem mass spectrometry platform that consisted of a Shimadzu Prominence UFLC XR high-performance liquid chromatograph (HPLC) (Shimadzu, Columbia, MD) coupled to an AB Sciex QTRAP® 5500 hybrid tandem quadrupole/linear ion trap mass spectrometer (AB Sciex, Framingham, MA). MetIQ software (Biocrates) controlled the assay workflow including sample registration, calculation of metabolite concentrations, and assay validation. A total of 182 analytes passed QC, with an additional 40 metabolite combinations derived from those analytes passed QC.

2.3.3 | Metabolomic nomenclature—Lipid notations listed as "Class CXX:Y" notate particular lipids indicating the XX total carbon number in the fatty acid chains and the Y number of double bonds. For example, PCaa C36:3 is phosphatidylcholine (PC) 36:3; i.e., a phosphatidylcholine with 36 total carbons among the two alkyl chains with 3 double bonds present. PC lipids listed as "PCaa" have both moieties at the sn-1 and sn-2 position as fatty acids bound to the glycerol backbone via ester bonds. PC lipids listed as "PCae" have one of the moieties, either the sn-1 or sn-2 position, as a fatty alcohol bound via an ether bond. For sphingomyelins (SM), the number of double bonds or the presence of a hydroxyl group (OH) are indicated for the fatty acid in the amide bond with the assumption that the backbone is sphingosine (d18:1). SFA refers to a sum of PC lipids containing fully saturated fatty acids (SFA), MUFA refers to a sum of PC lipids containing monounsaturated fatty acids (MUFA), and PUFA refers to a sum of PC lipids containing polyunsaturated fatty acids (PUFA). Lipid species measurements include potential isobaric and isomeric species.[39]

2.3.4 | Metabolomic bioinformatics—Statistical analyses were performed using the MetaboAnalyst web-based statistical package and GraphPad Prism (v 7.03, La Jolla, CA).[40–43] The data generated from the AbsoluteIDQ p180 kit which included analyte name and calculated concentration were imported into MetaboAnalyst for multivariate analysis. The metabolite data were normalized via autoscaling (mean-centered and divided by the standard deviation of each variable). Multivariate analysis included principal component analysis (PCA) and partial least square discriminate analysis (PLS-DA). The univariate analysis was performed in GraphPad Prism 7.03.

2.4 | Proteomics

2.4.1 | Proteomic sample preparation—Each cohort had $n = 10$ female mice aged 16.5 ± 4.0 months. Left and right ventricle tissues were homogenized in phosphate buffered saline using Precellys CK14 lysing kit (Bertin Corp., Rockville, MD). Proteins were extracted, purified from tissue lysates and trypsinolyzed and desalted as described previously.[44] Protein concentrations were measured by bicinchoninic acid assay and purified from tissue lysates by trichloroacetic acid precipitation.

2.4.2 | Liquid chromatography-tandem mass spectrometry data acquisition—Tryptic peptides were separated on a nano-ACQUITY UPLC analytical column (BEH130 C18, 1.7 μm, 75 μm × 200 mm, Waters) over a 165-min linear acetonitrile gradient (3%–40%) with 0.1% formic acid on a Waters nano-ACQUITY UPLC system and analyzed on a coupled Thermo Scientific Orbitrap Fusion Lumos Tribrid mass spectrometer as described previously.[45] Full scans were acquired at a resolution of 120 000 with an automatic gain control (AGC) target value of 10^6 and a maximum injection time of 50 ms. Precursors were selected for fragmentation by higher-energy collisional dissociation at a normalized collision energy of 32% for a maximum 3-s cycle. Products were analyzed in orbitrap at a resolution of 15 000 with an AGC target value of 10^3 or in ion trap with an AGC target value of 10^4 in parallel within a maximum injection time of 246 ms by applying an abundance dependent decision tree logic. Interrogated ions were dynamically excluded from reselection for 60 s.

2.4.3 | Liquid chromatography-tandem mass spectrometry data analysis—Tandem mass spectra were searched against a UniProt mouse reference proteome using a Sequest HT algorithm and a MS Amanda algorithm with a maximum precursor mass error tolerance of 10 ppm and a maximum product mass error tolerance of 0.5 Da in ion trap or 20 ppm in orbitrap, respectively.[46,47] Cysteine carbamidomethylation, asparagine/glutamine deamidation, and methionine oxidation were treated as static and dynamic modifications, respectively. Resulting hits were validated at a maximum false discovery rate of 0.01 using a semi-supervised machine learning algorithm Percolator.[48] Label-free quantifications were performed using Minora (Thermo Fisher Scientific), an aligned AMRT (Accurate Mass and Retention Time) cluster quantification algorithm. Abundance ratios were measured by comparing the MS1 peak volumes of peptide ions, whose identities were confirmed by MS2 sequencing as described above. Samples were normalized by total protein.

2.4.4 | Proteomic bioinformatics—Pathway and upstream regulator analysis were performed with Qiagen Ingenuity databases as described.[49] Proteins showing at least a

change (FC) of which $|z| \geq 1$ (standard score) with a false discovery rate (FDR) adjusted ANOVA p-value < .05 were considered significantly changed and used for further analysis. Ingenuity Pathway Analysis (IPA) was used to predict canonical pathways and upstream regulators according to the proteins that were significantly different using an absolute activation z-score of >2 for at least one condition with a Benjamini-Hochberg corrected Fisher's exact test p-value < .05.

2.4.5 | Proteomic data availability—The mass spectrometry proteomics data have been deposited to the ProteomeXchange Consortium via the PRIDE partner repository[50] with the dataset identifier PXD029349.

3 | RESULTS

3.1 | RA levels are decreased in *Rbp1*$^{-/-}$ mice hearts

RA, retinol, and retinyl esters (RE) were quantified in right (RV) and left (LV) ventricles of WT and *Rbp1*$^{-/-}$ mice using LC-MS/MS and HPLC-UV (Figure 1).[34–38,51] RA levels in *Rbp1*$^{-/-}$ mice were decreased by 33% ($p = .0017$) and 24% ($p = .032$) in LV and RV, respectively (Figure 1A). 9-cis-RA was not detectable above the LC-MS/MS assay limit of detection in biological matrices, which is 0.014 pmol/g. Retinol levels were decreased by 65% ($p = .0002$) and 69% ($p = .0001$) in LV compared to RV of WT and *Rbp1*$^{-/-}$ mice, respectively (Figure 1B). Total RE was similar between all tested genotypes and tissue regions (Figure 1C). Since RA is significantly decreased in *Rbp1*$^{-/-}$ mice hearts and is a known potent regulator of proper cellular function and tissue organization,[1] a multi-omics approach was developed to identify the global impact of reduced RA and reduced RA signaling in the adult heart.

3.2 | Unique metabolomic profiles of *Rbp1*$^{-/-}$*mice* hearts

The Biocrates AbsoluteIDQ p180 kit was used for high-throughput, targeted, quantitative metabolomics of multiple metabolite classes: acylcarnitines, amino acids, biogenic amines, glycerophospholipids, sphingolipids, and hexose. A total of 222 metabolite and metabolite combinations were analyzed for each cohort of Rbp1$^{-/-}$ and WT mice. Multivariate analysis was performed with MetaboAnalyst to identify metabolites that differ between WT and *Rbp1*$^{-/-}$ mice LV, RV, and atria (Figures 2 and S1–S4).[40,41] PLS-DA was used because its supervised nature better identifies features that define differences between two groups compared with PCA (Figures 2 and S1). PLS-DA plots were able to distinguish between WT and *Rbp1*$^{-/-}$ mice atria, RV and LV tissues (Figure 2A, R2 = 0.98, Q2 = 0.91, and Figure S1). In both WT and *Rbp1*$^{-/-}$ mice, LV and RV metabolites clustered together (Figure 2A). Metabolomic profiles of WT LV and RV were also compared to interrogate baseline ventricular differences (Figure S5).

Univariate analysis (Table 1, Figure S1) was able to identify 33 metabolites and metabolite combinations that had differential abundance between WT and *Rbp1*$^{-/-}$ (Table 1) ($p < .05$, false discovery rate <5%). Of those 33 metabolites, 21 were significantly different in RV, 24 in LV, and 15 in Atria (Table 1). Of these metabolites, 5 were acylcarnitines, 5 amino acids, 5 biogenic amines, 9 glycerophospholipids, and 2 sphingolipids. The acylcarnitines

were decreased in *Rbp1*$^{-/-}$ atria, LV and RV, compared to WT tissues. All amino acids, except aspartate were decreased in *Rbp1*$^{-/-}$ compared to WT in all three tissue regions. Two of the five biogenic amines, histamine and methionine sulfoxide, were decreased in *Rbp1*$^{-/-}$ atria compared to WT atria. While all significant biogenic amines except N-acetylornithine, were decreased in both LV and RV of *Rbp1*$^{-/-}$ compared to WT. Only 2 glycerophospholipids, lyso-phosphatidylcholine acyl C16:1 and lyso-phosphatidylcholine acyl C18:1, were decreased in all *Rbp1*$^{-/-}$ tissue types compared to WT. Both sphingolipids were increased in *Rbp1*$^{-/-}$ tissues compared to WT.

Pathway analysis was also performed with MetaboAnalyst to identify the most impacted pathways between WT and *Rbp1*$^{-/-}$ mice atria, left ventricle, and right ventricles (Figure 3, Table 2). Multiple amino acid biosynthesis and amino acid metabolism pathways were most significantly impacted in *Rbp1*$^{-/-}$ hearts compared to WT. Histidine metabolism and arginine biosynthesis pathways were significantly impacted in all three tissue regions.

3.3 | Unique proteomic profiles of *Rbp1*$^{-/-}$ hearts

The heart proteome in left and right ventricles of *Rbp1*$^{-/-}$ and WT mice was assessed via LC-MS/MS to identify proteins that were altered by reduced RA levels and reduced RA signaling. A total of 2606 unique proteins were quantified and protein abundance was compared between the right and left ventricles of WT and *Rbp1*$^{-/-}$ mouse hearts. Proteins with significantly altered abundances are shown in Figures 4, S6 and S7. A protein expression fold change FC >2-fold and FDR corrected ANOVA *p*-value cut off <.05 was used to identify significant changes in protein expression. A total of 340 proteins were differentially expressed between the tissue types. 48 proteins were downregulated, and 103 proteins were upregulated in *Rbp1*$^{-/-}$ RV compared to *Rbp1*$^{-/-}$ LV. 44 proteins were downregulated, and 103 proteins were upregulated in WT RV compared to WT LV. 75 proteins were downregulated, and 95 proteins were upregulated in *Rbp1*$^{-/-}$ RV compared to WT RV. 77 proteins were downregulated, and 90 proteins were upregulated in *Rbp1*$^{-/-}$ LV compared to WT LV.

Bioinformatic pathway analysis was also performed to provide further information about the impact of dysregulated RA signaling. Ingenuity Pathway Analysis (IPA) was used to predict canonical pathways and upstream regulators according to the proteins that were significantly different using an absolute activation *z*-score of >2 for at least one condition with a Benjamini-Hochberg corrected Fisher's exact test *p*-value < .05. The calculated *z*-score is a statistical measure of the match between expected relationship direction from published literature and observed gene expression from the experimental dataset and it is used to infer likely activation states of pathways or upstream regulators based on comparison with a model that assigns random regulation directions. Nine canonical pathways were significantly altered in the *Rbp1*$^{-/-}$ RV compared to WT RV, with all upregulated in *Rbp1*$^{-/-}$ RV except Integrin Signaling (Table 3). One canonical pathway, LXR/RXR Activation, was significantly upregulated in the *Rbp1*$^{-/-}$ LV compared to WT LV. Nine inferred upstream regulators were significantly activated (5) or inhibited (4) between the RV and LV of *Rbp1*$^{-/-}$ and WT mice (Table 4). IPA upstream regulator analysis, with a Benjamini-Hochberg corrected *p*-value < .01, was also to identify proteins that were significantly

associated with retinoic acid activity. In the left ventricle, sixteen proteins associated with retinoic acid activity were found to be significantly perturbed by loss of CRBP1, with 11 upregulated and 6 downregulated (Figure 5). In the right ventricle, ten proteins associated with retinoic acid activity were found to be significantly perturbed by loss of CRBP1, with 4 upregulated and 6 downregulated (Figure 6).

4 | DISCUSSION

Our present study investigated the metabolomic and proteomic differences between WT and *Rbp1*$^{-/-}$ mice hearts as well as their retinoid status. CRBP1 is important for maintaining retinoid homeostasis and retinoid quantification in heart was consistent with this function. RA levels were decreased in both the left and right ventricle of *Rbp1*$^{-/-}$ compared to WT mice, whereas ROL and Total RE values did not differ between the mice genotypes (Figure 1). This result is consistent with previous reports of decreased RA levels in *Rbp1*$^{-/-}$ tissues and is consistent with reduced RA biosynthesis.[31,32] Since the adult heart is responsive to RA and RA is essential for proper cellular function,[1,12] the decreased levels of RA in *Rbp1*$^{-/-}$ mice hearts would likely disrupt multiple pathways. Through metabolome and proteome analysis, the pathways that were most affected by ablation of *Rbp1* and disrupted cardiac RA signaling involved cellular metabolism and cardiac remodeling. The main metabolism pathways that were disrupted in *Rbp1*$^{-/-}$ mice included carnitine homeostasis, amino acid biosynthesis and metabolism, and LXR/RXR activation. The main cardiac remodeling pathways that were disrupted in *Rbp1*$^{-/-}$ mice included the Ras homolog gene family, member A (RhoA) signaling, Hippo, and Renin-Angiotensin pathways.

4.1 | Retinoid metabolism pathway

Whereas there were no differences in ROL and total RE levels between *Rbp1*$^{-/-}$ and WT, the amount of ROL is significantly decreased in the left ventricle of both *Rbp1*$^{-/-}$ and WT mice. Though steady state levels of RA were not different between LV and RV, the higher levels of retinol endow the RV with higher retinol precursor levels which may play a role in shaping local RA signaling. Of note, in addition to differences in physiology and repose to injury, the RV and LV are developmentally derived from different populations of myocardial progenitors.[4,52] Differences in metabolomic profiles of WT LV and RV are seen in Figure S5. Given that RA plays an important role in the anterior-posterior patterning of the heart,[53] we present here evidence of asymmetrical retinoid metabolism in the two cardiac regions that persists in the adult heart.

Of the proteins involved in retinoic acid biosynthesis, retinaldehyde dehydrogenase 1 (RALDH1) and retinol dehydrogenase 5 (RDH5) were detected in the proteomic analyses. RALDH1 catalyzes the oxidation of retinal to RA and was found at 1 and 1.4 times greater levels in the *Rbp1*$^{-/-}$ and WT mice right ventricle compared to the left ventricle, respectively.[1] Interestingly, RALDH1 has been shown to be downregulated in human heart failure.[54] However, previous publications have also shown RALDH1 levels can be inversely proportional to changes in RA.[55,56] Previous reports show intense expression of RDH5 in the heart,[57] but this protein was only found in left ventricles of both *Rbp1*$^{-/-}$ and WT

mice, which suggests that regionalization of retinoid enzyme expression might contribute to asymmetric retinoid metabolism in the heart.

Many proteins identified in the proteomic analysis contain a known or putative retinoic acid response element (RARE), like PTGDS and PDK4,[58,59] or are known RAR/RXR targets, like APOE,[60] and have altered expression between *Rbp1*$^{-/-}$ and WT mice. IPA upstream regulator analysis identified sixteen proteins in the left ventricle and ten proteins in the right ventricle that are associated with retinoic acid activity and were significantly perturbed by loss of CRBP1 (Figures 5 and 6, respectively). APOE and STAT1 were upregulated in both right and left ventricles and both proteins are further discussed below. KRT1 and KRT16 were downregulated in both right and left ventricles. RA has been shown to directly impact KRT1 mRNA stability.[61] KRT16 is induced with AP-1 activation, which is regulated by RA.[62] ITGB1 was downregulated in the right ventricle but upregulated in the left ventricle. ITGB1 is also present in 6 of the 9 canonical pathways altered in *Rbp1*$^{-/-}$ RV and the expression of ITGB1 is altered by RA.[63]

4.2 | Carnitine and lipid biosynthetic pathway

Carnitines are essential for transporting long-chain fatty acids into the mitochondrial matrix for metabolism.[64] In the heart, this reduces oxidative stress and inflammation, producing a cardioprotective effect.[65] Several studies have shown that supplementation with L-carnitine (levocarnitine, C0) can treat many cardiac problems, including ischemia-reperfusion injury, ventricular dysfunction, cardiac arrhythmia, and toxic myocardial injury.[65,66] In this study, C0 was significantly decreased in both the right and left ventricles of *Rbp1*$^{-/-}$ mice compared to WT mice (Table 1, Figures 2, S3 and S4). This decrease is likely attributed to a decrease in TMLHE, the enzyme responsible for the first step of carnitine biosynthesis, converting trimethyllysine into hydroxymethyllysine,[64] and had significantly decreased levels in the left ventricle of *Rbp1*$^{-/-}$ mice compared to left ventricle of WT mice. CPT1A, another protein in the carnitine biosynthetic pathway, was found in higher levels in the right ventricle of both *Rbp1*$^{-/-}$ and WT mice *(data not shown)*.[64] CPT1A is an important biomarker of diet-related metabolic alterations,[67,68] and has also been identified as a potential biomarker of heart disease detection.[69] Previous studies have shown that RA treatment activates fatty acid oxidation, leading to increased expression of *Cpt1a* expression.[70–72]

Our analysis also revealed differences in the levels of various phospholipid species. These differences were seen in comparing LV versus RV and also in comparing the two genotypes, *Rbp1*$^{-/-}$ and WT mice. Levels of unsaturated PC such as PC 34:2, 36:2, and 38:4 and PUFA in general were consistently higher in the RV versus LV of both WT and both *Rbp1*$^{-/-}$ mice and also in LV and RV of *Rbp1*$^{-/-}$ versus corresponding ventricle of WT mice. The right-left differential composition was also observed in both healthy and injured human hearts.[73]

4.3 | Amino acid biosyntehsisand metabolism

The heart is highly active, pumping over 6000 L of blood a day, and consumes large amounts of oxygen and metabolites for energy daily.[74] In instances of prolonged stress or ischemia, when oxygen and fatty acids levels decrease, the heart relies on other

molecules, such as amino acids, for energy.[74] Statistical analysis of our data identified a variety of amino acids and amino acid derivatives that were significantly different between *Rbp1*$^{-/-}$ and WT mice (Table 1, Figures 2 and S1–S4). Pathway analysis performed by MetaboAnalyst software also identified multiple amino acid biosynthesis and metabolism pathways that were changed between the *Rbp1*$^{-/-}$ and WT mice hearts (Figure 3, Table 2). Most of the top 5 most impacted pathways per tissue region (Table 2) are related to amino acid metabolism or biosynthesis. The pathway with the largest impact value calculated from pathway topology analysis was phenylalanine, tyrosine, and tryptophan biosynthesis (Impact:1, Figure 3). Studies have shown that these aromatic amino acids are not metabolized by a healthy heart and provide a strong marker of protein flux.[74] Histidine metabolism and arginine biosynthesis pathways were impacted in all three tissue types. Those two amino acids (as well as alanine, aspartate, glutamate, and glutamine) can be used by the oxygen-limited heart for energy.[74] The decrease levels of these amino acids could also be attributed to decreased proteolysis, a common occurrence in heart disease.[74] Branched-chain amino acid (BCAA) metabolism has been shown to be impaired in heart disease,[75,76] however, our results did not show any significant decreased levels of leucine, isoleucine, or valine.

4.4 | LXR/RXR activation

Liver X receptor/retinoid X receptor (LXR/RXR) signaling is essential for regulating lipid and glucose metabolism, inflammation, and cholesterol homeostasis.[77] Systemic LXR/RXR activation is also important for providing myocardial protection against many diseases, including atherosclerosis, hypertension, and diabetes.[77] Recently, several studies have established that dysregulated LXR/RXR activation was associated with heart disease.[78–80] LXR is activated by oxysterols and there were no oxysterols on our metabolomic panel. In this study, proteins related to the LXR/RXR activation pathway had altered levels in *Rbp1*$^{-/-}$ mice compared to WT mice, in both the left and right ventricles (Table 3). These proteins include APOE, SERPINA1, SERPINF1, and A1BG. APOE is a ligand for low density lipoprotein (LDL) receptors and plays important roles in cholesterol metabolism.[81] APOE can increase risk of heart disease,[81] and APOE levels were increased in the right and left ventricle of *Rbp1*$^{-/-}$ mice compared to WT. SERPIN1A is a serine protease inhibitor, which is essential for anti-inflammatory effects and SERPINA1 levels have been shown to be increased in chronic heart failure patients compared to healthy controls.[82] SERPINA1 has also been shown to promote tumorigenesis.[82] Therefore, SERPINA1 levels must be highly regulated for proper heart health. The proteomics data shows SERPIN1A levels were increased in the right and left ventricle of *Rbp1*$^{-/-}$ mice compared to WT. SERPINF1 is a secreted glycoprotein with antiangiogenic and antitumorigenic properties and SERPINF1 levels are increased in patients with metabolic syndrome and type 2 diabetes.[83] SERPINF1 has been shown to protect cardiac function after acute myocardial infarction through degradation of triglyceride.[83] The proteomics data shows SERPIN1F levels were increased in the right and left ventricle of *Rbp1*$^{-/-}$ mice compared to WT. A1BG is a member of the immunoglobulin family and while little is known of this protein's function, polymorphisms in the gene *A1BG* play a role in cardiovascular outcomes of patients response to antihypertensive medicine.[84] The proteomics data shows A1BG levels were increased in the right and left ventricle of *Rbp1*$^{-/-}$ mice compared to WT.

4.5 | Cardiac remodeling

RA levels are essential for proper cardiac remodeling. Insufficient RA leads to increased ventricular remodeling after injury, which negatively impacts heart function.[16] While these repair processes are necessary for cardiac regeneration after injury, they can easily become unchecked and lead to hypertrophy and, eventually, heart failure.[5,19] RA supplementation has even been studied as a promising therapeutic for attenuating ventricular remodeling after MI.[5,7,10,17,19–21] This therapeutic scheme is successful because of the many cardiac remodeling pathways regulated by RA, including RhoA, Hippo, and Renin-Angiotensin pathways.

4.5.1 | Ras homolog gene family, member A—RhoA is a small GTPase that plays important roles in embryonic development and regulates the actin cytoskeleton.[85] RhoA/Rho-associated protein kinase (ROCK) signaling regulates retinoid metabolism.[85] Additionally, RA promotes cytoskeletal remodeling of epicardial cells via the RhoA-signaling pathway, because RAR directly binds to RAREs within the promoters of Rho effectors.[5,7] Therefore, RhoA/ROCK signaling and RA is important for cardiac tissue regeneration after injury. In this study, the RhoA signaling pathway and the Signaling by Rho Family GTPases were both significantly altered in the right ventricle of *Rbp1*$^{-/-}$ mice compared to WT mice (Table 3). Additionally, three proteins involved in RhoA signaling were dysregulated between the two mice populations in both ventricles. MYLK3 was downregulated in both right and left ventricle of *Rbp1*$^{-/-}$ mice compared to WT. MYL7 existed in higher levels in both right and left ventricle of *Rbp1*$^{-/-}$ mice compared to WT. ITGB1 was downregulated in the right ventricle but upregulated in the left ventricle of *Rbp1*$^{-/-}$ mice compared to WT.

4.5.2 | Hippo signaling pathway—The Hippo signaling pathway controls organ size by regulating cell proliferation and apoptosis, and is important for cardiac fibroblast development.[86] The Hippo effectors YAP and TAZ directly affect expression levels of DHRS3, a retinal reductase with expression inversely related to RA levels. The Hippo pathway was not identified as significantly impacted in the proteomic pathway analysis, but two proteins involved in the pathway, MYH7 and NPPA, were dysregulated between the mice populations (Figure 5). MYH7 is expected to be upregulated during RA deficiency,[87] and was increased in the left ventricle of *Rbp1*$^{-/-}$ mice compared to WT. NPPA is regulated by RAR/RXR,[88] and was found at decreased levels in the left ventricle of *Rbp1*$^{-/-}$ mice, but increased levels of right ventricle compared to WT.

4.5.3 | Renin-angiotensin system—Renin-angiotensin system (RAS) regulates blood pressure and volume, and RAS plays important roles in many cardiovascular disorders.[89] In instances of hemodynamic overload, RAS becomes active and this leads to myocyte hypertrophy and fibrosis.[19] Unresolved hypertrophy and cardiac remodeling cause heart failure. Studies have shown that RA signaling prevents cardiac remodeling by inhibiting RAS, which halted the hypertrophy to heart failure conversion.[19,90] While this pathway was not identified as significantly impacted during the proteomic pathway analysis, many individual proteins (collagen, CAMK2A, and LAMA3) involved in RAS and hypertrophy were significantly altered between *Rbp1*$^{-/-}$ and WT mice. Collagen, including COL1A2 and

COL4A1 (Figure 5), lead to changes in the extra cellular matrix and RA has been shown to increase their gene expression.[91–93] Collagen was found in larger amounts in *Rbp1*$^{-/-}$ left ventricle compared to WT left ventricle. CAMK2A leads to cardiomyopathy and RA has been shown to regulate CAMK2A activation.[13,14,22,91,94] Camk2a levels are increased in failing hearts.[91] CAMK2A was found at higher concentrations in the left ventricle compared to right ventricle in both *Rbp1*$^{-/-}$ and WT mice. LAMA3 is an extracellular matrix protein important for RAS signaling and RA increases its gene expression.[95] LAMA3 was found at higher concentrations in right ventricle of *Rbp1*$^{-/-}$ mice compared to right ventricle of WT. In a study of acute pressure overload in rats, angiotensin II activates the JAK/STAT pathway.[96] STAT1 is upregulated in both the right and left ventricles of *Rbp1*$^{-/-}$ mice and was identified as a top upstream regulator disrupted by CRBP1 loss (Figures 5 and 6). STAT1 protein levels are modulated by RA.[97]

4.6 | Conclusion

This study provides a systems biology analysis regarding RA homeostasis in the adult mouse heart. *Rbp1*$^{-/-}$ mice were used as a model of reduced RA in adult mice. Overall, this study elucidates that RA remains essential in the adult heart, especially in pathways related to metabolism and cardiac remodeling. Dysregulation of the retinoid pathway of *Rbp1*$^{-/-}$ mice hearts was examined through quantitation of retinoids, including RA, the active form of Vitamin A. Through a targeted metabolomics approach, 33 metabolites significantly affected by loss of CRBP1 and disrupted retinoic acid signaling were identified. The most significantly affected pathways included amino acid biosynthesis and metabolism. Through an untargeted mass-spectrometry approach, 340 proteins significantly perturbed by loss of CRBP1 and disrupted retinoic acid signaling were identified. The most significantly affected canonical pathways included LXR/RXR activation, actin cytoskeleton signaling, PAK signaling, and RhoA signaling.

This study provides valuable metabolomic and proteomic data but includes some limitations. Our proteomic methodology is a direct sampling technique with limitations in the detectable range. Proteins of lower abundance may be present or possibly changed but may not be detected due to abundance. Metabolites are limited to those contained in the Biocrates AbsoluteIDQ p180 kit, which is a subset of the whole metabolomic profile. The Biocrates kit has only been validated for plasma, but it has been previously used by us and by other groups for analyzing heart tissue.[98–101] Hearts were not perfused upon collection consistent with other studies in the literature using the Biocrates kit for analysis of heart tissue,[98–100] however it is possible blood contained within the tissue contributes signal towards the total protein and metabolite content. Samples were limited to availability of animals at the time, and future studies would be necessary to inform on any metabolomic and/or proteomic gender or age differences in *Rbp1*$^{-/-}$ mice. WT and *Rbp1*$^{-/-}$ mice were not littermates and derived from independently bred lines. All mice were fed a normal diet, and previous studies have shown no differences between WT and *Rbp1*$^{-/-}$ mice food consumption and body weight on this diet, but differences in adiposity and retinoid metabolites have been seen in *Rbp1*$^{-/-}$ mice fed a high-fat or vitamin a deficient diet.[51,102] This study may be useful in developing a molecular classification of heart disease through targeted analysis coupled with absolute quantitation of proteins and metabolites which could potentially represent markers

for different forms and stages of heart disease. Finally, by using an adult genetic model of decreased RA, this study provides information about the effects of reduced RA on adult hearts while avoiding the confounding effects of dietary vitamin A deficiency.

Supplementary Material

Refer to Web version on PubMed Central for supplementary material.

ACKNOWLEDGEMENTS

This work was supported by R01HD077260 (MAK, ARM) and T32 GM066706 (AED) from the National Institutes of Health, and in part by the University of Maryland Baltimore, School of Pharmacy Mass Spectrometry Center (SOP1841-IQB2014)

Funding information

HHS | NIH | Eunice Kennedy Shriver National Institute of Child Health and Human Development (NICHD), Grant/Award Number: R01HD077260; HHS | NIH | National Institute of General Medical Sciences (NIGMS), Grant/Award Number: T32 GM066706; University of Maryland Baltimore, School of Pharmacy Mass Spectrometry Center, Grant/Award Number: SOP1841-IQB2014

DATA AVAILABILITY STATEMENT

The data that support this study are openly available at the ProteomeXchange Consortium via the PRIDE partner repository at (https://www.ebi.ac.uk/pride/archive/) with the dataset identifier PXD029349.

Abbreviations:

AA	amino acids
AC	acylcarnitines
APCI	atmospheric pressure chemical ionization
BA	biogenic amines
BCAA	branched-chain amino acids
C0	levocarntine, L-carnitine
CRBP1	cellular-retinol binding protein, type 1
FC	fold change
FDR	false discovery rate
FIA	flow injection analysis
HPLC	high-performance liquid chromatography
IPA	ingenuity pathway analysis
LC-MRM^3	liquid chromatography-multistage-tandem mass spectrometry

LC-MS/MS	liquid chromatography-tandem mass spectrometry
LDL	low density lipoprotein
LV	left ventricle
LXR/RXR	liver X receptor/retinoid X receptor
MI	myocardial infarction
MUFA	sum of PC lipids containing monounsaturated fatty acids
OH	hydroxyl group
PC	glycerophospholipids
PC	phosphatidylcholine
PCA	principal component analysis
PLS-DA	partial least square discriminate analysis
PUFA	sum of PC lipids containing polyunsaturated fatty acids
QC	quality control
RA	*all-trans-retinoic* acid
RAR/RXR	retinoic acid receptor/retinoid x receptor
RARE	retinoic acid response element
Rbp1 $^{-/-}$	cellular retinol-binding protein, type 1 *(Rbp1)* knockout mice
RE	retinyl esters
RhoA	Ras homolog gene family, member A
ROCK	RhoA/Rho-associated protein kinase
RV	right ventricle
SFA	sum of PC lipids containing fully saturated fatty acids
SM	sphingolipids
SM	sphingomyelins
TAZ	tafazzin
YAP	yes-associated protein

REFERENCES

1. Napoli JL. Physiological insights into all-trans-retinoic acid biosynthesis. Biochim Biophys Acta. 2012;1821(1):152–167. [PubMed: 21621639]
2. Napoli JL. Retinoic acid biosynthesis and metabolism. FASEB J. 1996;10(9):993–1001. [PubMed: 8801182]
3. Napoli JL. Retinoic acid: its biosynthesis and metabolism. Prog Nucleic Acid Res Mol Biol. 1999;63:139–188. [PubMed: 10506831]
4. Xavier-Neto J, Sousa Costa ÂM, Figueira ACM, et al. Signaling through retinoic acid receptors in cardiac development: doing the right things at the right times. Biochim Biophys Acta. 2015;1849(2):94–111. [PubMed: 25134739]
5. Wang S, Yu J, Jones JW, et al. Retinoic acid signaling promotes the cytoskeletal rearrangement of embryonic epicardial cells. FASEB J. 2018;32(7):3765–3781. [PubMed: 29447006]
6. Wang S, Huang W, Castillo HA, et al. Alterations in retinoic acid signaling affect the development of the mouse coronary vasculature. Dev Dyn. 2018;247(8):976–991. [PubMed: 29806219]
7. Wang S, Yu J, Kane MA, Moise AR. Modulation of retinoid signaling: therapeutic opportunities in organ fibrosis and repair. Pharmacol Ther. 2020;205:107415. [PubMed: 31629008]
8. Gavrilova R, Babovic N, Lteif A, et al. Vitamin A deficiency in an infant with PAGOD syndrome. Am J Med Genet A. 2009;149A(10):2241–2247. [PubMed: 19760653]
9. Clagett-Dame M, DeLuca HF. The role of vitamin A in mammalian reproduction and embryonic development. Annu Rev Nutr. 2002;22:347–381. [PubMed: 12055350]
10. Pan J, Baker KM. Retinoic acid and the heart. Vitam Horm. 2007;75:257–283. [PubMed: 17368319]
11. Zhu S, Guleria RS, Thomas CM, et al. Loss of myocardial retinoic acid receptor α induces diastolic dysfunction by promoting intracellular oxidative stress and calcium mishandling in adult mice. J Mol Cell Cardiol. 2016;99:100–112. [PubMed: 27539860]
12. Asson-Batres MA, Ryzhov S, Tikhomirov O, et al. Effects of vitamin A deficiency in the postnatal mouse heart: role of hepatic retinoid stores. Am J Physiol Heart Circ Physiol. 2016;310(11):H1773–H1789. [PubMed: 27084391]
13. Park SW, Nhieu J, Lin Y-W, Wei L-N. All-trans retinoic acid attenuates isoproterenol-induced cardiac dysfunction through Crabp1 to dampen CaMKII activation. Eur J Pharmacol. 2019;858:172485. [PubMed: 31238067]
14. Park SW, Persaud SD, Ogokeh S, Meyers TA, Townsend D, Wei L-N. CRABP1 protects the heart from isoproterenol-induced acute and chronic remodeling. J Endocrinol. 2018;236(3):151–165. [PubMed: 29371236]
15. Liu Y, Chen H, Mu DI, et al. Association of serum retinoic acid with risk of mortality in patients with coronary artery disease. Circ Res. 2016;119(4):557–563. [PubMed: 27323773]
16. Minicucci MF, Azevedo PS, Oliveira SA Jr, et al. Tissue vitamin A insufficiency results in adverse ventricular remodeling after experimental myocardial infarction. Cell Physiol Biochem. 2010;26(4–5):523–530. [PubMed: 21063090]
17. Freire CMM, Azevedo PS, Minicucci MF, et al. Influence of different doses of retinoic acid on cardiac remodeling. Nutrition. 2011;27(7):824–828. [PubMed: 21035307]
18. Choudhary R, Baker KM, Pan J. All-trans retinoic acid prevents angiotensin II- and mechanical stretch-induced reactive oxygen species generation and cardiomyocyte apoptosis. J Cell Physiol. 2008;215(1):172–181. [PubMed: 17941088]
19. Choudhary R, Palm-Leis A, Scott RC, et al. All-trans retinoic acid prevents development of cardiac remodeling in aortic banded rats by inhibiting the renin-angiotensin system. Am J Physiol Heart Circ Physiol. 2008;294(2):H633–H644. [PubMed: 18156191]
20. de Paiva SAR, Zornoff LAM, Okoshi MP, et al. Ventricular remodeling induced by retinoic acid supplementation in adult rats. Am J Physiol Heart Circ Physiol. 2003;284(6):H2242–H2246. [PubMed: 12574000]

21. Paiva SAR, Matsubara LS, Matsubara BB, et al. Retinoic acid supplementation attenuates ventricular remodeling after myocardial infarction in rats. J Nutr. 2005;135(10):2326–2328. [PubMed: 16177190]
22. Nagpal I, Wei L-N. All-trans retinoic acid as a versatile cytosolic signal modulator mediated by CRABP1. Int J Mol Sci. 2019;20(15):3610.
23. Napoli JL. Cellular retinoid binding-proteins, CRBP, CRABP, FABP5: effects on retinoid metabolism, function and related diseases. Pharmacol Ther. 2017;173:19–33. [PubMed: 28132904]
24. Boerman MHEM Napoli JL. Cellular retinol-binding protein-supported retinoic acid synthesis relative roles of microsomes and cytosol. J Biol Chem. 1996;271(10):5610–5616. [PubMed: 8621422]
25. Cremona O, Muda M, Appel RD, et al. Differential protein expression in aortic smooth muscle cells cultured from newborn and aged rats. Exp Cell Res. 1995;217(2):280–287. [PubMed: 7698227]
26. Miano Joseph M, Topouzis S, Majesky Mark W, Olson EN. Retinoid receptor expression and all-trans retinoic acid-mediated growth inhibition in vascular smooth muscle cells. Circulation. 1996;93(10):1886–1895. [PubMed: 8635268]
27. Xu G, Redard M, Gabbiani G, Neuville P. Cellular retinol-binding protein-1 is transiently expressed in granulation tissue fibroblasts and differentially expressed in fibroblasts cultured from different organs. Am J Pathol. 1997;151(6):1741–1749. [PubMed: 9403724]
28. Neuville P, Geinoz A, Benzonana G, et al. Cellular retinol-binding protein-1 is expressed by distinct subsets of rat arterial smooth muscle cells in vitro and in vivo. Am J Pathol. 1997;150(2):509–521. [PubMed: 9033267]
29. Yu M, Ishibashi-Ueda H, Ohta-Ogo K, et al. Transient expression of cellular retinol-binding protein-1 during cardiac repair after myocardial infarction. Pathol Int. 2012;62(4):246–253. [PubMed: 22449228]
30. Neuville P, Yan Z-Q, Gidlöf A, et al. Retinoic acid regulates arterial smooth muscle cell proliferation and phenotypic features in vivo and in vitro through an RARα-dependent signaling pathway. Arterioscler Thromb Vasc Biol. 1999;19(6):1430–1436. [PubMed: 10364073]
31. Pierzchalski K, Taylor RN, Nezhat C, et al. Retinoic acid biosynthesis is impaired in human and murine endometriosis. Biol Reprod. 2014;91(4):84. [PubMed: 25143356]
32. Pierzchalski K, Yu J, Norman V, Kane MA. CrbpI regulates mammary retinoic acid homeostasis and the mammary microenvironment. FASEB J. 2013;27(5):1904–1916. [PubMed: 23362116]
33. Ghyselinck NB, Båvik C, Sapin V, et al. Cellular retinol-binding protein I is essential for vitamin A homeostasis. EMBO J. 1999;18(18):4903–4914. [PubMed: 10487743]
34. Kane MA, Chen N, Sparks S, Napoli JL. Quantification of endogenous retinoic acid in limited biological samples by LC/MS/MS. Biochem J. 2005;388(Pt 1):363–369. [PubMed: 15628969]
35. Kane MA, Folias AE, Wang C, Napoli JL. Quantitative profiling of endogenous retinoic acid in vivo and in vitro by tandem mass spectrometry. Anal Chem. 2008;80(5):1702–1708. [PubMed: 18251521]
36. Kane MA, Napoli JL. Quantification of endogenous retinoids. Methods Mol Biol. 2010;652:1–54. [PubMed: 20552420]
37. Jones JW, Pierzchalski K, Yu J, Kane MA. Use of fast HPLC multiple reaction monitoring cubed for endogenous retinoic acid quantification in complex matrices. Anal Chem. 2015;87(6):3222–3230. [PubMed: 25704261]
38. Kane MA, Folias AE, Napoli JL. HPLC/UV quantitation of retinal, retinol, and retinyl esters in serum and tissues. Anal Biochem. 2008;378(1):71–79. [PubMed: 18410739]
39. Biocrates. Annotation of potential isobaric and isomeric lipid species measured with AbsoluteIDQ p180 Kit (and p150 Kit). 2017;2(35017).
40. Xia J, Wishart DS. Using MetaboAnalyst 3.0 for comprehensive metabolomics data analysis. Curr Protoc Bioinformatics. 2016;55(1):14.10.11–14.10.91.
41. Xia J, Sinelnikov IV, Han B, Wishart DS. MetaboAnalyst 3.0—making metabolomics more meaningful. Nucleic Acids Res. 2015;43(W1):W251–W257. [PubMed: 25897128]

42. Chong J, Soufan O, Li C, et al. MetaboAnalyst 4.0: towards more transparent and integrative metabolomics analysis. Nucleic Acids Res. 2018;46(W1):W486–W494. [PubMed: 29762782]
43. Chong J, Wishart DS, Xia J. Using MetaboAnalyst 4.0 for comprehensive and integrative metabolomics data analysis. Curr Protoc Bioinformatics. 2019;68(1):e86. [PubMed: 31756036]
44. Huang W, Yu J, Liu T, et al. Proteomic evaluation of the natural history of the acute radiation syndrome of the gastrointestinal tract in a non-human primate model of partial-body irradiation with minimal bone marrow sparing includes dysregulation of the retinoid pathway. Health Phys. 2020;119(5):604–620. [PubMed: 32947489]
45. Huang W, Yu J, Liu T, et al. Proteomics of non-human primate plasma after partial-body radiation with minimal bone marrow sparing. Health Phys. 2020;119(5):621–632. [PubMed: 32947488]
46. Eng JK, Fischer B, Grossmann J, MacCoss MJ. A fast SEQUEST cross correlation algorithm. J Proteome Res. 2008;7(10):4598–4602. [PubMed: 18774840]
47. Dorfer V, Pichler P, Stranzl T, et al. MS Amanda, a universal identification algorithm optimized for high accuracy tandem mass spectra. J Proteome Res. 2014;13(8):3679–3684. [PubMed: 24909410]
48. Käll L, Canterbury JD, Weston J, Noble WS, MacCoss MJ. Semi-supervised learning for peptide identification from shotgun proteomics datasets. Nat Methods. 2007;4(11):923–925. [PubMed: 17952086]
49. Krämer A, Green J, Pollard J, Tugendreich S. Causal analysis approaches in ingenuity pathway analysis. Bioinformatics. 2014;30(4):523–530. [PubMed: 24336805]
50. Perez-Riverol Y, Csordas A, Bai J, et al. The PRIDE database and related tools and resources in 2019: improving support for quantification data. Nucleic Acids Res. 2019;47(D1):D442–D450. [PubMed: 30395289]
51. Kane MA, Folias AE, Pingitore A, et al. CrbpI modulates glucose homeostasis and pancreas 9-cis-retinoic acid concentrations. Mol Cell Biol. 2011;31(16):3277–3285. [PubMed: 21670153]
52. Zaffran S, Kelly RG, Meilhac SM, Buckingham ME, Brown NA. Right ventricular myocardium derives from the anterior heart field. Circ Res. 2004;95(3):261–268. [PubMed: 15217909]
53. Hochgreb T, Linhares VL, Menezes DC, et al. A caudorostral wave of RALDH2 conveys anteroposterior information to the cardiac field. Development. 2003;130(22):5363–5374. [PubMed: 13129847]
54. Yang NI, Parker LE, Yu J, et al. Cardiac retinoic acid levels decline in heart failure. JCI Insight. 2021;6(8):e137593.
55. Kane MA, Folias AE, Wang C, Napoli JL. Ethanol elevates physiological all-trans-retinoic acid levels in select loci through altering retinoid metabolism in multiple loci: a potential mechanism of ethanol toxicity. FASEB J. 2010;24(3):823–832. [PubMed: 19890016]
56. Posch KC, Burns RD, Napoli JL. Biosynthesis of all-trans-retinoic acid from retinal. Recognition of retinal bound to cellular retinol binding protein (type I) as substrate by a purified cytosolic dehydrogenase. J Biol Chem. 1992;267(27):19676–19682. [PubMed: 1527087]
57. Wang J, Chai X, Eriksson U, Napoli JL. Activity of human 11-cis-retinol dehydrogenase (Rdh5) with steroids and retinoids and expression of its mRNA in extra-ocular human tissue. Biochem J. 1999;338 (Pt 1):23–27. [PubMed: 9931293]
58. Balmer JE, Blomhoff R. Gene expression regulation by retinoic acid. J Lipid Res. 2002;43(11):1773–1808. [PubMed: 12401878]
59. Distel E, Cadoudal T, Collinet M, Park EA, Benelli C, Bortoli S. Early induction of pyruvate dehydrogenase kinase 4 by retinoic acids in adipocytes. Mol Nutr Food Res. 2017;61(5):1600920.
60. Goodman AB. Retinoid receptors, transporters, and metabolizers as therapeutic targets in late onset Alzheimer disease. J Cell Physiol. 2006;209(3):598–603. [PubMed: 17001693]
61. Aldehlawi H, Usman S, Lalli A, et al. Serum lipids, retinoic acid and phenol red differentially regulate expression of keratins K1, K10 and K2 in cultured keratinocytes. Sci Rep. 2020;10(1):4829. [PubMed: 32179842]
62. Törmä H Regulation of keratin expression by retinoids. Dermatoendocrinol. 2011;3(3):136–140. [PubMed: 22110773]
63. Zirn B, Samans B, Spangenberg C, Graf N, Eilers M, Gessler M. All-trans retinoic acid treatment of Wilms tumor cells reverses expression of genes associated with high risk and relapse in vivo. Oncogene. 2005;24(33):5246–5251. [PubMed: 15897880]

64. Adeva-Andany MM, Calvo-Castro I, Fernández-Fernández C, Donapetry-Garcia C, Pedre-Piñeiro AM. Significance of l-carnitine for human health. IUBMB Life. 2017;69(8):578–594. [PubMed: 28653367]

65. Wang Z-Y, Liu Y-Y, Liu G-H, Lu H-B, Mao C-Y. l-Carnitine and heart disease. Life Sci. 2018;194:88–97. [PubMed: 29241711]

66. Ferrari R, Merli E, Cicchitelli G, Mele D, Fucili A, Ceconi C. Therapeutic effects of l-carnitine and propionyl-l-carnitine on cardiovascular diseases: a review. Ann N Y Acad Sci. 2004;1033(1):79–91. [PubMed: 15591005]

67. Díaz-Rúa R, Palou A, Oliver P. Cpt1a gene expression in peripheral blood mononuclear cells as an early biomarker of diet-related metabolic alterations. Food Nutr Res. 2016;60:33554. [PubMed: 27885970]

68. Sánchez J, Priego T, Picó C, et al. Blood cells as a source of transcriptional biomarkers of childhood obesity and its related metabolic alterations: results of the IDEFICS study. J Clin Endocrinol Metab. 2012;97(4):E648–E652. [PubMed: 22278432]

69. Irvin MR, Aslibekyan S, Hidalgo B, Arnett D. CPT1A: the future of heart disease detection and personalized medicine? Clin Lipidol. 2014;9(1):9–12. [PubMed: 25774225]

70. Cifre M, Palou A, Oliver P. Impaired CPT1A gene expression response to retinoic acid treatment in human PBMC as predictor of metabolic risk. Nutrients. 2020;12(8):2269.

71. Amengual J, Petrov P, Bonet ML, Ribot J, Palou A. Induction of carnitine palmitoyl transferase 1 and fatty acid oxidation by retinoic acid in HepG2 cells. Int J Biochem Cell Biol. 2012;44(11):2019–2027. [PubMed: 22871568]

72. Mercader J, Ribot J, Murano I, et al. Remodeling of white adipose tissue after retinoic acid administration in mice. Endocrinology. 2006;147(11):5325–5332. [PubMed: 16840543]

73. Samouillan V, Martinez de Lejarza Samper IM, Benitez Amaro A, et al. Biophysical and lipidomic biomarkers of cardiac remodeling post-myocardial infarction in humans. Biomolecules. 2020;10(11):1471.

74. Drake KJ, Sidorov VY, McGuinness OP, Wasserman DH, Wikswo JP. Amino acids as metabolic substrates during cardiac ischemia. Exp Biol Med. 2012;237(12):1369–1378.

75. Huang Y, Zhou M, Sun H, Wang Y. Branched-chain amino acid metabolism in heart disease: an epiphenomenon or a real culprit? Cardiovasc Res. 2011;90(2):220–223. [PubMed: 21502372]

76. Yang N, Parker L, Yu J, et al. Retinoic acid depletion in the failing heart. JCI. 2020;In Revision.

77. Cannon MV, van Gilst WH, de Boer RA. Emerging role of liver X receptors in cardiac pathophysiology and heart failure. Basic Res Cardiol. 2016;111(1):3. [PubMed: 26611207]

78. DeLeon-Pennell KY, Mouton AJ, Ero OK, et al. LXR/RXR signaling and neutrophil phenotype following myocardial infarction classify sex differences in remodeling. Basic Res Cardiol. 2018;113(5):40. [PubMed: 30132266]

79. Sun H, Wang D, Liu D, et al. Differential urinary proteins to diagnose coronary heart disease based on iTRAQ quantitative proteomics. Anal Bioanal Chem. 2019;411(11):2273–2282. [PubMed: 30806752]

80. Lin Y-S, Chang T-H, Shi C-S, et al. Liver X receptor/retinoid X receptor pathway plays a regulatory role in pacing-induced cardiomyopathy. J Am Heart Assoc. 2019;8(1):e009146. [PubMed: 30612502]

81. Mahley RW. Apolipoprotein E: from cardiovascular disease to neurodegenerative disorders. J Mol Med. 2016;94:739–746. [PubMed: 27277824]

82. Kitsis RN, Riquelme JA, Lavandero S. Heart disease and cancer—are the two killers colluding? Circulation. 2018;138(7):692–695. [PubMed: 30359137]

83. Zhang H, Sun T, Jiang X, et al. PEDF and PEDF-derived peptide 44mer stimulate cardiac triglyceride degradation via ATGL. J Transl Med. 2015;13:68. [PubMed: 25890298]

84. McDonough CW, Gong Y, Padmanabhan S, et al. Pharmacogenomic association of non-synonymous SNPs in SIGLEC12, A1BG and the selectin region and cardiovascular outcomes. Hypertension. 2013;62(1):48–54. [PubMed: 23690342]

85. García-Mariscal A, Peyrollier K, Basse A, et al. RhoA controls retinoid signaling by ROCK dependent regulation of retinol metabolism. Small GTPases. 2016;9(5):433–444. [PubMed: 27754752]

86. Xiao Y, Hill MC, Zhang M, et al. Hippo signaling plays an essential role in cell state transitions during cardiac fibroblast development. Dev Cell. 2018;45(2):153–169.e156. [PubMed: 29689192]
87. Paschaki M, Schneider C, Rhinn M, et al. Transcriptomic analysis of murine embryos lacking endogenous retinoic acid signaling. PLoS One. 2013;8(4):e62274. [PubMed: 23638021]
88. Stefanovic S, Zaffran S. Mechanisms of retinoic acid signaling during cardiogenesis. Mech Dev. 2017;143:9–19. [PubMed: 28007475]
89. Wollert KC, Drexler H. The renin-angiotensin system and experimental heart failure. Cardiovasc Res. 1999;43(4):838–849. [PubMed: 10615411]
90. Wang H-J, Zhu Y-C, Yao T Effects of all-trans retinoic acid on angiotensin II-induced myocyte hypertrophy. J Appl Physiol. 2002;92(5):2162–2168. [PubMed: 11960970]
91. Kehat I, Molkentin JD. Molecular pathways underlying cardiac remodeling during pathophysiologic stimulation. Circulation. 2010;122(25):2727–2735. [PubMed: 21173361]
92. Sanchez M, Gionti E, Arcella A, Pontarelli G, De Lorenzo F. Alpha 2(I) collagen gene expression is up-regulated in quail chondrocytes pretreated with retinoic acid. Biochem J. 1993;295(Pt 1):115–119. [PubMed: 8216205]
93. Malik M, Webb J, Catherino WH. Retinoic acid treatment of human leiomyoma cells transformed the cell phenotype to one strongly resembling myometrial cells. Clin Endocrinol. 2008;69(3):462–470.
94. Chen J, Kelly PT. Retinoic acid stimulates alpha-CAMKII gene expression in PC12 cells at a distinct transcription initiation site. J Neurosci. 1996;16(18):5704–5714. [PubMed: 8795626]
95. Wong YF, Wilson PD, Unwin RJ, et al. Retinoic acid receptor-dependent, cell-autonomous, endogenous retinoic acid signaling and its target genes in mouse collecting duct cells. PLoS One. 2012;7(9):e45725. [PubMed: 23049847]
96. Pan J, Fukuda K, Kodama H, et al. Role of angiotensin II in activation of the JAK/STAT pathway induced by acute pressure overload in the rat heart. Circ Res. 1997;81(4):611–617. [PubMed: 9314843]
97. Gianni M, Terao M, Fortino I, et al. Stat1 is induced and activated by all-trans retinoic acid in acute promyelocytic leukemia cells. Blood. 1997;89(3):1001–1012. [PubMed: 9028332]
98. Schnackenberg LK, Pence L, Vijay V, et al. Early metabolomics changes in heart and plasma during chronic doxorubicin treatment in B6C3F1 mice. J Appl Toxicol. 2016;36(11):1486–1495. [PubMed: 26934058]
99. Halade GV, Kain V, Tourki B, Jadapalli JK. Lipoxygenase drives lipidomic and metabolic reprogramming in ischemic heart failure. Metabolism. 2019;96:22–32. [PubMed: 30999004]
100. Mao K, Quipildor GF, Tabrizian T, et al. Late-life targeting of the IGF-1 receptor improves healthspan and lifespan in female mice. Nat Commun. 2018;9(1):2394. [PubMed: 29921922]
101. Zalesak-Kravec S, Huang W, Wang P, et al. Multi-omic analysis of non-human primate heart after partial-body radiation with minimal bone marrow sparing. Health Phys. 2021;121(4):352–371. [PubMed: 34546217]
102. Zizola CF, Frey SK, Jitngarmkusol S, Kadereit B, Yan N, Vogel S. Cellular retinol-binding protein type I (CRBP-I) regulates adipogenesis. Mol Cell Biol. 2010;30(14):3412–3420. [PubMed: 20498279]

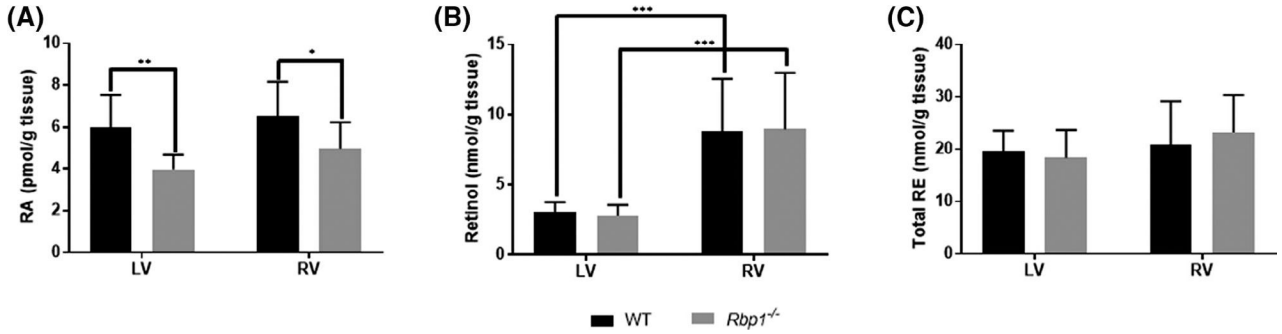

FIGURE 1.

Quantitation of retinoid metabolites in left ventricle (LV) and right ventricle (RV) of WT and *Rbp1*$^{-/-}$ mice. (A) RA levels are reduced in LV and RV of *Rbp1*$^{-/-}$ compared to WT. (B) Retinol levels were decreased in both WT and *Rbp1*$^{-/-}$ mice LV compared to RV. (C) RE levels were statistically unchanged between mice population and tissue type. Error bars represent standard deviation. **p*-value < .05, ***p*-value < .01, and ****p*-value < .001 as determined by an unpaired Student's *t*-test. Data is mean ± SEM; $n = 10$ each genotype

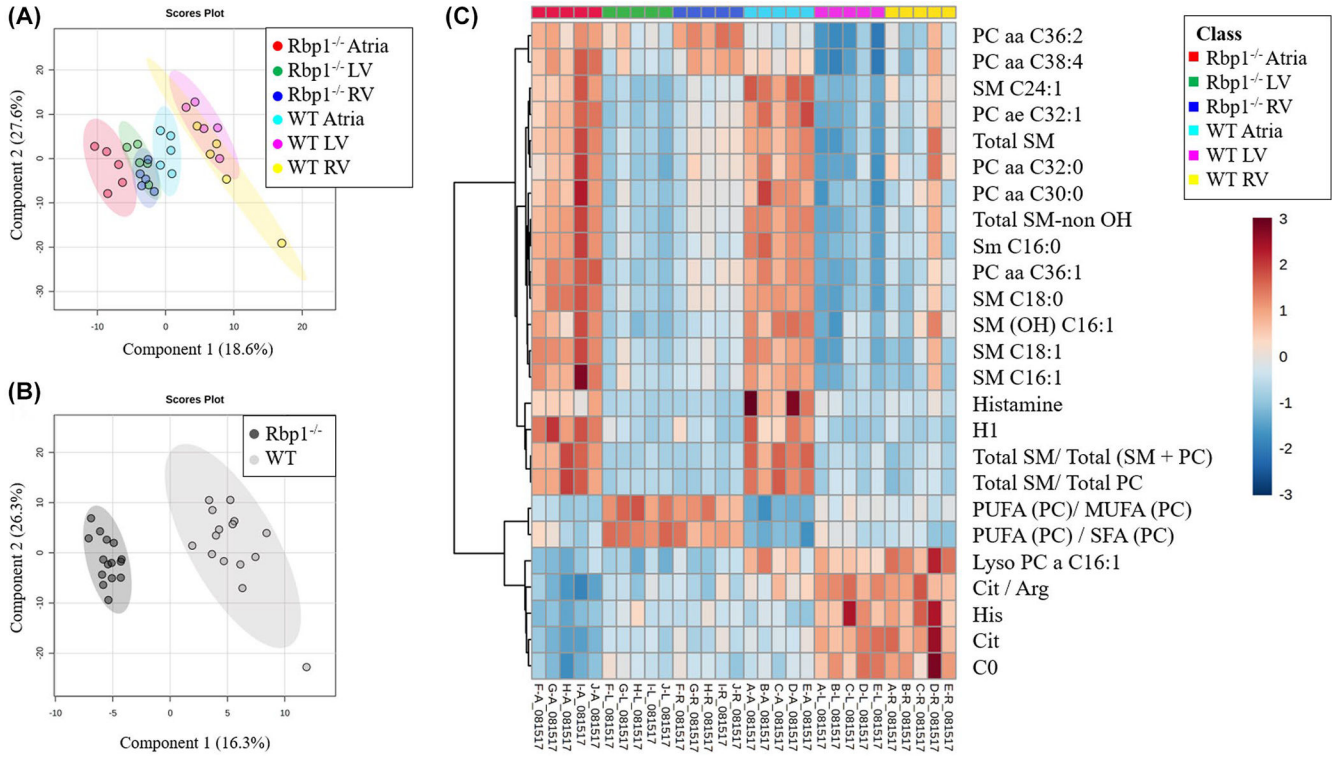

FIGURE 2.

Multivariate analysis and hierarchical clustering displays statistical metabolite differences between WT and *Rbp1*$^{-/-}$ mice atria, LV and RV. (A) PLS-DA plot comparing *Rbp1*$^{-/-}$ Atria (Red), *Rbp1*$^{-/-}$ LV (Green), *Rbp1*$^{-/-}$ RV (Blue), WT Atria (Cyan), WT LV (Magenta), WT RV (Yellow). R2 = 0.98. Q2 = 0.91. *N* = 5 per group. Each point represents a data set from an individual animal tissue. The 95% confidence intervals are indicated by elliptical patterns per group. (B) PLS-DA plot comparing all *Rbp1*$^{-/-}$ samples (black) and WT samples (gray). R2 = 0.99. Q2 = 0.96. *n* = 15 per group. The 95% confidence intervals are indicated by elliptical patterns per group. (C) Heatmap displaying the top 25 metabolites based on t-test/ANOVA, Euclidean distancing, and Ward clustering

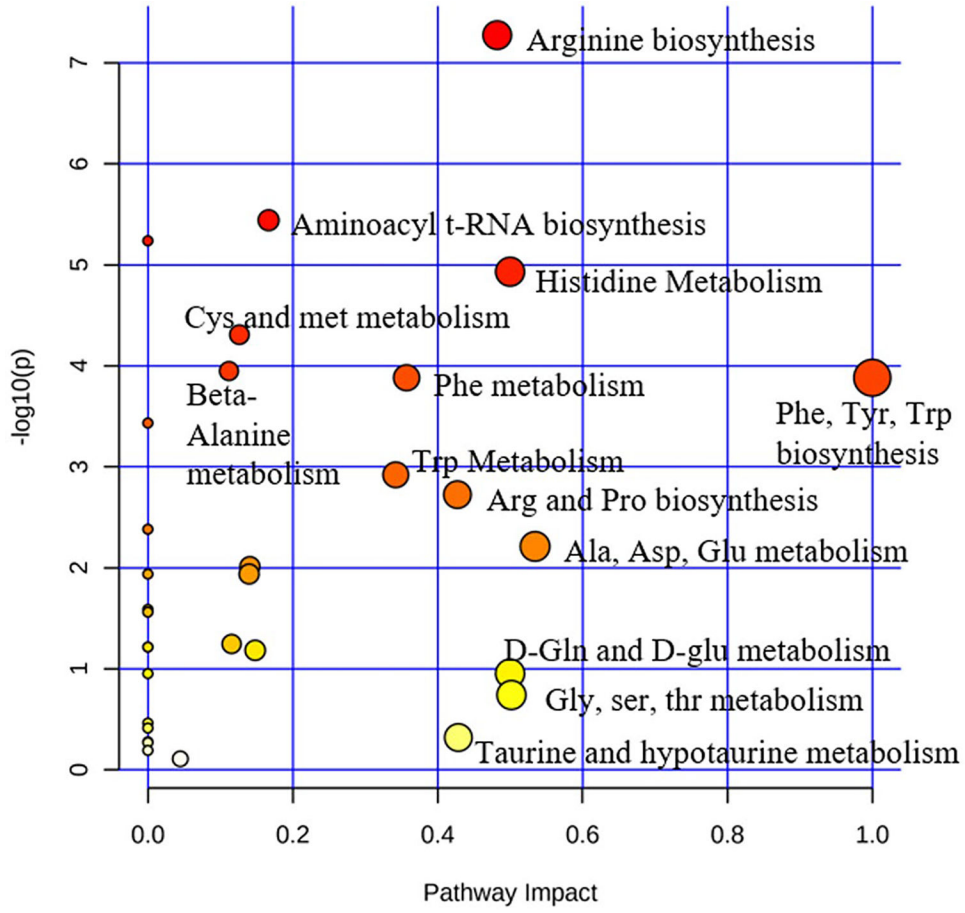

FIGURE 3.

Pathway analysis of metabolites differentially expressed in WT compared to *Rbp1*$^{-/-}$ mice hearts. Atria, LV, and RV tissues were grouped together for WT and *Rbp1*$^{-/-}$ mice

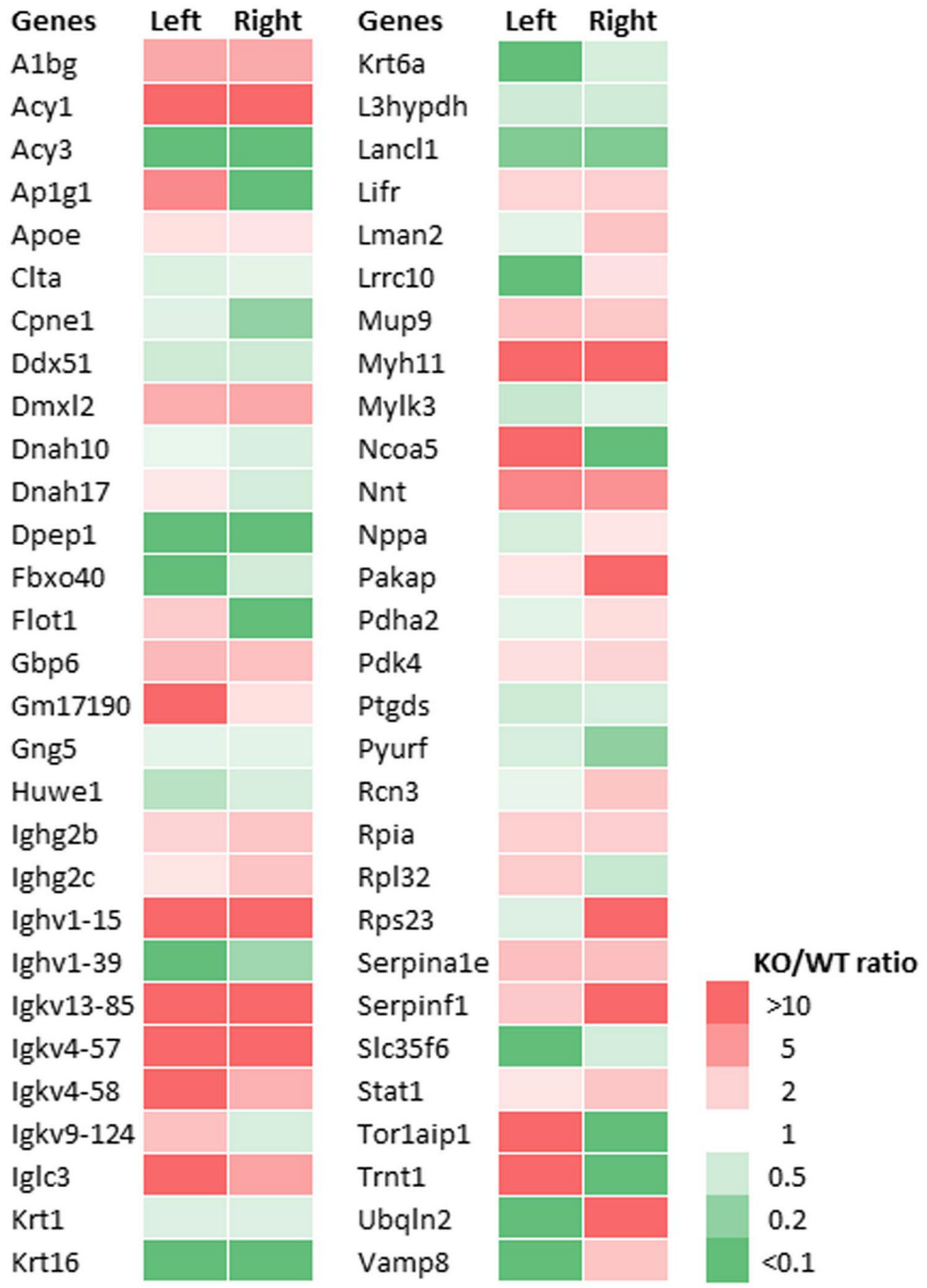

FIGURE 4.

Expression of proteins most changed in both left and right ventricles of *Rbp1*$^{-/-}$ mice compared to WT. Minimum 2-fold change and FDR adjusted *p*-value < .05 were criteria for inclusion

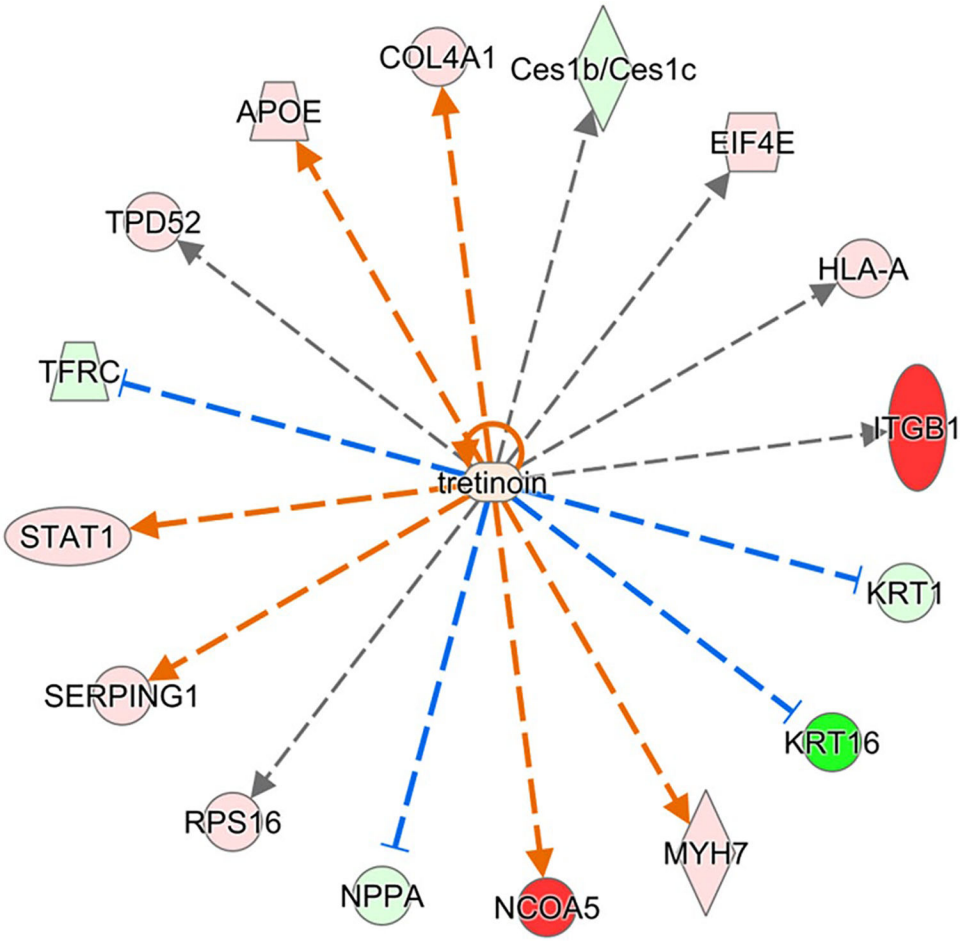

FIGURE 5.

Proteins in left ventricle regulated by retinoic acid and significantly perturbed in *Rbp1*$^{-/-}$. Proteins with minimum 2-fold change and FDR adjusted *p*-value < .05 were selected for upstream regulator interference at a cutoff of Benjamini-Hochberg adjusted Fisher's exact test *p*-value < .01. Red color indicates significant upregulation and green indicates downregulation, with intensity of color corresponding to magnitude of upregulation

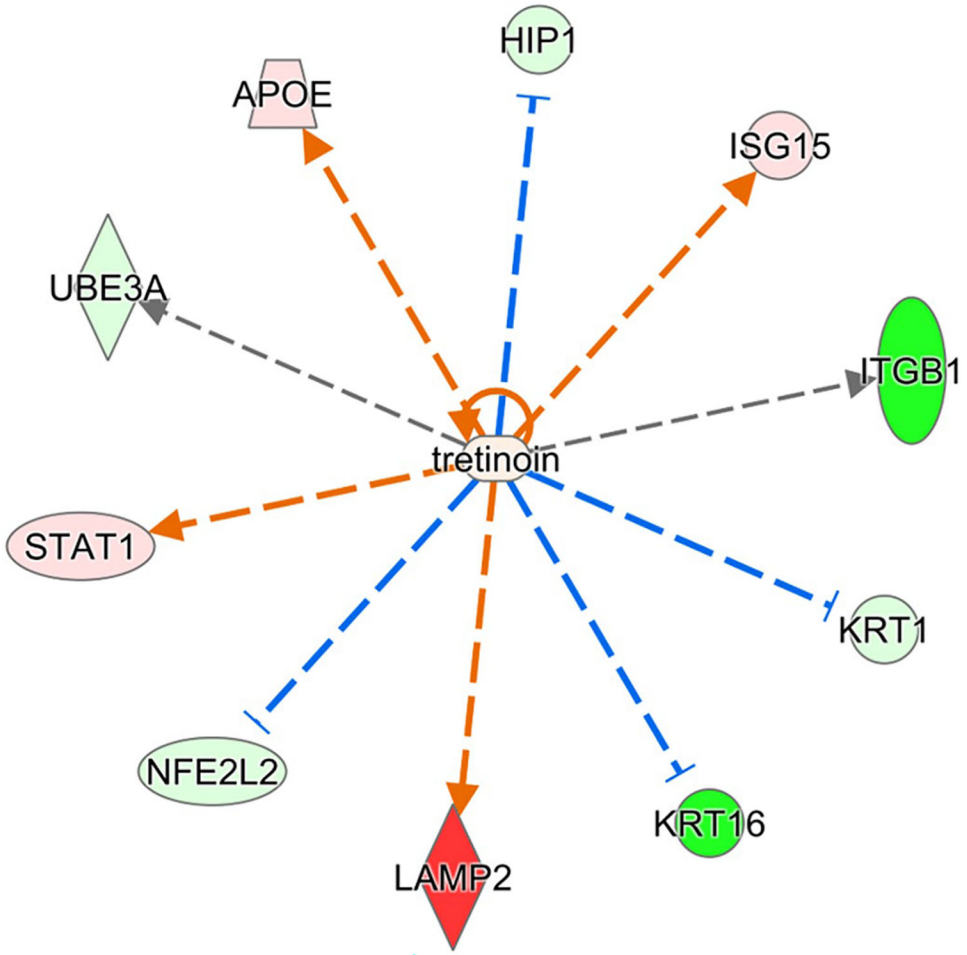

FIGURE 6.

Proteins in right ventricle regulated by retinoic acid and significantly perturbed in *Rbp1*$^{-/-}$. Proteins with minimum 2-fold change and FDR adjusted *p*-value < .05 were selected for upstream regulator interference at a cutoff of Benjamini-Hochberg adjusted Fisher's exact test *p*-value < .01. Red color indicates significant upregulation and green indicates downregulation, with intensity of color corresponding to magnitude of upregulation

TABLE 1

Metabolites significantly changed between WT and *Rbpl1*$^{-/-}$ atria, left ventricle (lv), and right ventricle (RV)

		Atria					Left ventricle					Right ventricle				
			WT atria		Rbpl$^{-/-}$ Atria			WT LV		Rbpl$^{-/-}$ LV			WT RV		Rbpl$^{-/-}$ RV	
Metabolite	**Class**	***p* Value**	**Mean**	**SD**	**Mean**	**SD**	***p* Value**	**Mean**	**SD**	**Mean**	**SD**	***p* Value**	**Mean**	**SD**	**Mean**	**SD**
C0	AC	.005	542.20	59.2	375.00	79.4	.001	853.80	101.4	569.00	67.4	.006	902.40	204.6	537.60	78.6
C14	AC	.171	1.96	0.7	1.48	0.1	.128	2.04	0.7	1.48	0.3	.046	2.05	0.7	1.34	0.2
C18:l	AC	.301	1.90	0.9	1.15	0.3	.154	2.26	1.0	1.09	0.2	.071	2.19	1.1	0.98	0.2
C18:l-OH	AC	.100	2.06	1.2	1.18	0.1	.030	2.66	1.1	1.23	0.2	.043	2.60	1.2	1.21	0.2
C3-DC (C4-OH)	AC	.032	12.90	4.3	7.70	1.2	.063	14.20	5.1	9.14	1.3	.089	14.94	6.0	9.60	1.3
Asp	AA	.0001	1562.40	323.8	3044.40	328.6	.020	1383.60	475.1	2504.40	718.1	.065	1405.20	632.1	2134.80	428.9
Cit	AA	.0002	177.60	16.8	104.24	18.0	.00003	275.80	26.1	160.40	14.7	.002	295.00	55.1	168.60	25.9
His	AA	.018	211.80	27.8	170.40	13.9	.006	354.40	63.0	240.80	29.5	.002	367.20	63.4	235.40	20.7
Met	AA	.030	143.60	35.1	100.88	8.8	.005	145.20	30.9	89.12	11.8	.015	163.40	50.2	94.08	5.3
Orn	AA	.171	13.88	3.7	11.34	1.0	.070	11.71	4.2	7.42	1.9	.040	12.34	4.5	6.53	2.7
Ac-Orn	BA	.002	6.38	1.2	10.38	1.5	.008	7.78	1.9	13.80	3.3	.156	9.29	3.9	13.72	5.0
Carnosine	BA	.019	34.48	2.7	54.06	14.6	.045	35.86	6.0	26.48	6.5	.095	39.14	9.5	27.40	10.2
Histamine	BA	.031	13.50	4.6	7.90	1.6	.037	4.24	1.0	3.01	0.4	.011	4.55	1.1	2.83	0.4
Met-SO	BA	.013	5.07	1.5	2.88	0.4	.002	4.00	0.8	2.07	0.6	.036	4.57	1.6	2.65	0.6
Spermidine	BA	.009	4.47	0.8	6.74	1.2	.410	9.81	2.4	8.66	1.7	.323	6.81	2.0	5.78	0.9
lysoPC a C16:l	PC	.001	1.48	0.2	0.91	0.1	.0001	1.47	0.1	0.94	0.1	.000	1.80	0.2	1.05	0.1
lysoPC a C18:l	PC	.030	17.02	5.1	10.64	1.8	.001	14.14	1.4	9.94	1.1	.010	17.80	3.4	11.58	2.3
PC aa C34:2	PC	.113	945.40	109.2	1077.80	125.4	.009	733.40	169.6	1126.00	191.9	.065	1180.20	235.1	1421.60	92.5
PC aa C36:l	PC	.226	355.80	28.2	388.20	47.4	.027	64.14	33.0	117.02	28.6	.253	173.64	61.3	212.60	35.4
PC aa C36:2	PC	.001	668.00	55.7	940.40	102.7	.001	300.80	122.0	715.40	129.9	.002	633.80	184.7	1034.60	64.4
PC aa C38:3	PC	.139	79.72	17.3	95.38	12.4	.010	32.24	16.0	61.36	11.0	.148	77.14	32.7	102.64	13.9
PC aa C38:4	PC	.011	1054.60	68.5	1322.80	168.2	.004	439.40	170.1	858.40	156.3	.039	877.20	251.9	1205.40	157.6
PC ae C38:2	PC	.142	13.30	1.0	16.00	3.6	.009	5.61	2.4	10.81	2.4	.130	13.38	4.9	18.00	3.6
PC ae C40:4	PC	.504	16.58	1.2	18.02	4.4	.038	7.18	3.1	11.39	2.2	.492	15.50	5.5	17.66	3.8
SM C20:2	SM	.008	0.78	0.1	1.10	0.2	.002	0.49	0.2	0.98	0.2	.033	0.82	0.3	1.29	0.3
SM C22:3	SM	.003	11.52	2.6	20.20	3.9	.0002	8.13	2.6	19.40	2.9	.009	13.27	5.9	24.44	4.3

		Atria					Left ventricle					Right ventricle				
			WT atria		$Rbpl^{-/-}$ Atria			WT LV		$Rbpl^{-/-}$ LV			WT RV		$Rbpl^{-/-}$ RV	
Metabolite	**Class**	***p* Value**	**Mean**	**SD**	**Mean**	**SD**	***p* Value**	**Mean**	**SD**	**Mean**	**SD**	***p* Value**	**Mean**	**SD**	**Mean**	**SD**
(C2+C3)/C0	AC	.008	0.50	0.1	0.78	0.2	.002	0.24	0.04	0.50	0.1	.010	0.26	0.1	0.64	0.2
C2/C0	AC	.008	0.49	0.1	0.76	0.2	.002	0.23	0.04	0.49	0.1	.010	0.26	0.1	0.62	0.2
Cit/Arg	AA	.0002	1.49	0.2	0.82	0.2	.00001	1.92	0.1	1.18	0.1	.001	1.85	0.2	1.19	0.2
Orn/Arg	AA	.079	0.12	0.03	0.088	0.003	.084	0.082	0.03	0.054	0.01	.049	0.08	0.03	0.045	0.02
Total AC/C0	AC	.009	0.59	0.1	0.89	0.2	.002	0.30	0.1	0.58	0.1	.010	0.32	0.1	0.71	0.2
Total AC-OH/Total AC	AC	.140	0.033	0.01	0.023	0.004	.008	0.046	0.01	0.025	0.004	.012	0.042	0.01	0.022	0.01
Total lysoPC/Total PC	PC	.008	0.019	0.002	0.015	0.001	.010	0.026	0.01	0.017	0.002	.019	0.018	0.002	0.014	0.002

Note: Metabolites assayed $Rbpl^{-/-}$ and WT mice, $n = 5$ each genotype.

Abbreviations: AC, acylcarnitine; AA, amino acids; BA, biogenic amines; PC, glycerophospholipids; SM, sphingolipids.

TABLE 2

Pathway analysis of metabolites differentially expressed in WT compared to *Rbp1*$^{-/-}$ mice hearts

Pathway	Hits	Raw *p*	Holm adjust	FDR	Impact
Atria					
Histidine metabolism	5/16	5.45E–05	0.0017	0.0012	0.4999
Arginine biosynthesis	7/14	9.69E–05	0.0030	0.0012	0.4822
Nicotinate and nicotinamide metabolism	1/15	.0001	0.0033	0.0012	0
Pantothenate and CoA biosynthesis	2/19	.0007	0.0189	0.0052	0
Aminoacyl-tRNA biosynthesis	19/48	.0010	0.0268	0.0061	0.1667
Left ventricle					
Histidine metabolism	5/16	.0007	0.0222	0.0155	0.4999
Arginine biosynthesis	7/14	.0010	0.0306	0.0155	0.4822
beta-Alanine metabolism	5/21	.0014	0.0435	0.0155	0.1119
Aminoacyl-tRNA biosynthesis	19/48	.0021	0.0611	0.0169	0.1667
Cysteine and methionine metabolism	2/33	.0108	0.3019	0.0689	0.1263
Right ventricle					
beta-Alanine metabolism	5/21	.0015	0.0495	0.0367	0.1119
Histidine metabolism	5/16	.0028	0.0870	0.0367	0.4999
Arginine biosynthesis	7/14	.0034	0.1033	0.0367	0.4822
Phenylalanine, tyrosine and tryptophan biosynthesis	2/4	.0071	0.2045	0.0451	1
Phenylalanine metabolism	2/12	.0071	0.2045	0.0451	0.3571

Note: Samples are arranged according to *p* value, and the top 5 most impacted pathways by tissue type, based on *p* value, were included. Hits refers to the number of matched metabolites from the uploaded data, over the total number of compounds in the pathways. Raw p is the original *p* value calculated from the enrichment analysis. Holm p is the *p* value adjusted by Holm-Bonferroni method. The FDR p is the *p* value adjusted using False Discovery Rate. Impact is the pathway impact value calculated from pathway topology analysis. Results were normalized via Autoscaling (mean-centered and divided by the standard deviation of each variable). Pathway Enrichment Analysis was Global Test. Pathway Topology Analysis was Relative-betweenness Centrality. Pathway library was Mus musculus (KEGG).

TABLE 3

Canonical pathways altered in *Rbp1*$^{-/-}$ right and left ventricle

Canonical pathways	Ventricle	B-H *p*-value	Activation *z*-score	Proteins
LXR/RXR activation	Left	.009	1.6	C4A/C4B, APOE, SERPINF1, SERPINA1, SERPINF2, A1BG
LXR/RXR activation	Right	.0003	1.9	APOE, PON1, FASN, C9, AMBP, SERPINF1, SERPINA1, A1BG
Actin cytoskeleton signaling	Right	.01	0.8	RAP1B, ITGB1, CRKL, MYLK3, MYL4, MYLK, MYH11, MYL7
PAK signaling	Right	.03	1.3	RAP1B, ITGB1, MYL4, MYLK, MYL7
RhoA signaling	Right	.03	2.2	SEPT9, MYLK3, MYL4, MYLK, MYL7
Phospholipase C signaling	Right	.03	0.4	RAP1B, ITGB1, GNG2, MYL4, GNG5, Ighg2b, MYL7
Signaling by Rho family GTPases	Right	.03	1.3	ITGB1, SEPT9, GNG2, MYL4, MYLK, GNG5, MYL7
Production of nitric oxide and reactive oxygen species in macrophages	Right	.04	1.3	RAP1B, PON1, APOE, PPP2R2A, SERPINA1, STAT1
Regulation of actin-based motility by Rho	Right	.05	1.0	ITGB1, MYL4, MYLK, MYL7
Integrin signaling	Right	.05	−0.8	RAP1B, ITGB1, CRKL, MYLK3, MYLK, MYL7

Note: Criteria for pathways changes were a nonzero absolute activation *z*-score and a Benjamini-Hochberg corrected Fisher's exact test *p*-value < .01.

TABLE 4

Upstream regulators altered in *Rbp1*$^{-/-}$ right and left ventricle

Upstream regulator	Activation *z*-score	B-H corrected *p*-value	Genes regulated by upstream regulator
Left ventricle *Rbp1*$^{-/-}$ vs. left ventricle WT			
Bvht	1.982	.0403	Hbb-b2, HBG2, MYH7, SERPINF1
Right ventricle *Rbp1*$^{-/-}$ vs. right ventricle WT			
Ifnar	2.219	.0354	B2M, GBP2, ISG15, STAT1, TAPBP
NRAS	−1.912	.0238	AKAP12, B2M, GBP2, ISG15, NPPA, OSBPL1A, PKIA, STAT1
HEY2	−1.956	.0238	MYH11, MYL4, MYL7, NPPA
PNPT1	−2	.0354	GBP2, GBP6, ISG15, STAT1
STAT6	−2.087	.0093	APOE, COBLL1, FASN, GBP2, GBP6, Ighg2b, ISG15, LIFR, PDK4, PLBD1, RAB35, SERPINA1, SERPINF1
WT right ventricle vs WT left ventricle			
GATA1	2.397	.012	Ahsp, ALOX12, GP1BA, GP1BB, GP9, Hbb-b2, NHP2, PF4, SNCA, TGFB1I1
FLNA	1.964	.0072	GP1BA, GP1BB, GP9, ITGB1
Rbp1$^{-/-}$ right ventricle vs *Rbp1*$^{-/-}$ left ventricle			
GATA1	2.575	.0006	Ahsp, ALOX12, CNN3, GP1BA, GP1BB, GP9, Hbb-b2, NHP2, NPPA, PF4, PLEK, TGFB1I1

Note: Criteria for upstream regulator interference were a nonzero absolute activation *z*-score and a Benjamini-Hochberg corrected Fisher's exact test *p*-value < .01.